

Spontaneous Formation of Inorganic Helical Fibers and Rings

Oscar Giraldo,[†] Manuel Marquez,^{†,||} Stephanie L. Brock,[†] Steven L. Suib,^{*,†,‡} Hugh Hillhouse,[§] and Michael Tsapatsis[§]

Contribution from the U-60, Department of Chemistry, University of Connecticut, Storrs, Connecticut 06269-3060, Department of Chemical Engineering, and Institute of Materials Science, University of Massachusetts, Amherst, Massachusetts 01003-3110, Department of Chemical Engineering, 159 Goessmann Laboratory, University of Massachusetts, Amherst, Massachusetts 01003-3110, and Los Alamos National Lab, Chemical Science and Technology Division, CST-DO, Los Alamos, New Mexico 87545

Received May 30, 2000

Abstract: Helical fibers of porous manganese oxide have been prepared from colloidal solutions. Such fibers have diameters ranging from several mm to the micrometer range. These helices are formed, starting from a well-mixed colloidal precursor and applying no external forcing other than its confinement in a capillary or beaker and heating for a period of time. Structural changes occur during gelation, leading from an amorphous to a layered structure. The layered structure can be ion-exchanged with hard cation template ions and then heated to form tunnel structure materials that retain the helical morphology. The helices are semiconductors and permeable. As the concentration of the colloidal precursor is lowered, helices are no longer formed, but instead, two-dimensional rings are produced. The formation process of these helices is related to contraction of the gel during heating with capillary pressure until solvent is removed followed by expansion of the helix.

I. Introduction

Preparation of inorganic films, wires, helices, rings, and regular patterns^{1–14} have intrigued researchers over the past 100 years and have led to numerous experimental and theoretical studies. Porous inorganic materials have also been intensely pursued to generate media that can be used for control of host–guest interactions,^{1–3} for shape selectivity,⁴ and for understanding fundamental phenomena such as diffusion and adsorption. Generation of well-ordered macroscopic, mesoscopic, and microscopic materials such as reproducible inorganic helices has been an elusive goal, especially when specific physical properties such as porosity or conductivity are of interest. Here we show that well-formed durable inorganic helices that are permeable, porous, and conducting can be readily synthesized, isolated, and functionalized. This approach may be generalized to other inorganic and organometallic systems.

Pursuit of new conducting wires and thin films via molecular engineering has recently been the focus of several laboratories for potential applications as sensors,¹ to enhance computing speed and storage density of electronic materials,² and as effective membranes for separations.³ Entrapment of carbon and organic conducting polymeric materials¹ or vapor deposition in porous media like zeolites⁴ have produced wires; however, removal of such materials from hosts has been elusive. Conducting organic wires having donor acceptor moieties linked by bridges have recently been reported.⁵

Organic helical structures occur at the macromolecular and molecular levels and are widely found throughout nature.⁶ However, purely inorganic helices have only recently been observed.⁷ Transition metal arsenate and germanate zeolite-like systems have been shown to have helical 3-D pores.⁸ Chemical vapor deposition methods have been used to coat carbon to produce 10–15 μm diameter inorganic ceramic spirals. Helices of MCM-41 type materials have been observed for silicate systems.⁹ Spun fibers, spray-dried hollow spheres,¹⁰ and large-pore mesoporous silica fibers¹¹ ($\sim 10 \mu\text{m}$) have been synthesized. Interfacial control has led to formation of fibers of 50–1000 μm in length.¹² Helical mesoporous silica fibers¹³ and layered

* To whom correspondence should be addressed. E-mail: suib@uconnvm.uconn.edu.

[†] University of Connecticut.

[‡] Department of Chemical Engineering and Institute of Materials Science, University of Massachusetts.

[§] Department of Chemical Engineering, 159 Goessmann Laboratory, University of Massachusetts.

^{||} Los Alamos National Lab.

(1) (a) Wu, C. G.; Bein, T. *Science* **1994**, *264*, 1757–1759. (b) Marquez, M.; Larsen, G.; Haller, G. L. *J. Phys. Chem.* **1992**, *96*, 4145–4149.

(2) Trau, M.; Yao, N.; Kim, E.; Xia, Y.; Whitesides, G. M.; Aksay, I. A. *Nature* **1997**, *390*, 674–676.

(3) den Exter, M. J.; Jansen, J. C.; van de Graaf, J. M.; Kapteijn, F.; Moulijn, J. A.; van Bekkum, H. In *Recent Advances and New Horizons in Zeolite Science and Technology*; Chon, H., Ed.; Studies in Surface Science and Catalysis, Vol. 102; Elsevier: New York, 1996; pp 413–454.

(4) Jones, C. W.; Tsuji, K.; Davis, M. E. *Nature* **1998**, *393*, 52–54.

(5) Davis, W. B.; Svec, W. A.; Ratner, M. A.; Wasielewski, M. R. *Nature* **1998**, *396*, 60–63.

(6) Rowan, A. E.; Nolte, R. J. M. *Angew. Chem., Int. Ed.* **1998**, *37*, 63–68.

(7) Soghomonian, V.; Chen, Q.; Haushalter, R. C.; Zubieta, J.; O'Connor, C. J.; Lee, Y. S. *Science* **1993**, *259*, 1596–1599.

(8) Gier, T. E.; Bu, X.; Feng, P.; Stucky, G. D. *Nature* **1998**, *395*, 154–157.

(9) Raimondi, M. E.; Maschmeyer, T.; Templer, R. H.; Seddon, J. M. *J. Chem. Soc. Chem. Comm.* **1997**, 1843–1844.

(10) Bruinsma, P. J.; Kim, A. Y.; Liu, J.; Baskaran, S. *Chem. Mater.* **1997**, *9*, 2507–2512.

(11) Yang, P.; Zhao, D.; Chmelka, B. F.; Stucky, G. D. *Chem. Mater.* **1998**, *10*, 2033–2036.

(12) Schacht, S.; Huo, Q.; Voigt-Martin, I. G.; Stucky, G. D.; Schuth, F. *Science* **1996**, *273*, 768–771.

(13) (a) Huo, Q.; Zhao, D.; Feng, J.; Weston, K.; Buratto, S. K.; Stucky, G. D.; Schacht, S.; Schuth, F. *Adv. Mater.* **1997**, *9*, 974–978. (b) Yang, M.; Sokolov, I.; Coombs, N.; Kresge, C. T.; Ozin, G. A. *Adv. Mater.* **1999**, *11*, 1427–1431.

(14) Akiyama, Y.; Mizukami, F.; Kiyozumi, Y.; Maeda, K.; Izutsu, H.; Sakaguchi, K. *Angew. Chem., Int. Ed.* **1999**, *38*, 1420–1422.

silicates¹⁴ have also been produced. Ring stains and deposits and mechanisms of formation have recently been related to capillary flow effects.¹⁵

Large-pore semicrystalline mesoporous transition metal oxides of manganese oxide¹⁶ and other transition metals¹⁷ have been reported. Recently, disk-shaped crown ether phthalocyanine and polysiloxane coiled-coil aggregates, of 50 nm diameter and a few micrometers in length, have been grown in organic gels.¹⁸ Filaments of single crystalline Ga a few cm in length and on the order of 2–100 μm diameter have recently been reported to grow via de-intercalation of Cr_2GaN .¹⁹ The above systems are difficult to isolate, form in the midst of other morphologies, are difficult to functionalize, or are insulating.

We have recently reported the ability to reproducibly prepare well-defined helical filaments of porous manganese oxide.²⁰ These materials are semiconductors, contain micropores, and can be altered to form other structures and compositions that are the focus of this manuscript. The starting sol materials contain an organic cation, which results in gels that form helices. Helices are produced when using high concentrations of sol, and rings form when such sols are diluted.

II. Experimental Section

A. Synthesis. A colloidal solution of lamellar manganese oxide (0.1 M in Mn) was prepared by adding 10 mol $[\text{N}(\text{CH}_3)_4]\text{MnO}_4$ to a stirred mixture of 100 mL of distilled deionized water and 30 mL of 2-butanol at room temperature. After 30 min a dark red–brown solution was formed in the lower aqueous layer. This aqueous solution was separated from the upper organic layer with a separatory funnel and then either used as-is or diluted (down to 0.001 M in Mn). The resultant colloids when placed in capillaries and heated at 85 °C for 160 h (3 mm i.d. capillary tubes) form helical fibers at high concentrations of the initial sols or ring patterns at low concentrations.

The synthesized fibers were ion-exchanged with K^+ for preparation of synthetic birnessite, K-OL-1. The ion-exchange reaction was carried out at room temperature by immersing the helices in a 1 M solution of KNO_3 under ultrasound for 10 min followed by an extensive washing step with deionized water. Heating the K-OL-1 helix to 500 °C in air leads to formation of a tunnel structure K-OMS-2 helix.

Characterization. Structural analysis was done with a Scintag 2000 PDS system with $\text{Cu K}\alpha$ radiation at a 1.5406 Å wavelength. Step scans of 0.03° were used. An X-ray beam voltage of 45 kV and a current of 40 mA were used. Scans were collected from 5° to 80° 2θ . High-resolution transmission electron micrographs were obtained by imaging ultrathin sections on carbon mesh copper grids using a JEOL 2010 microscope operated at an accelerating voltage of 200 kV. The samples were set in LR White hard-grade acrylic resin obtained from the London Resin Company. The resin/sample blocks were sectioned using a Sorvall Porter-Blum MT-2B ultra-microtome and Diatome diamond knife. The samples were then imaged on a JEOL 2000FX operated at an accelerating voltage of 200 kV.

In addition, the morphology was observed with optical microscopy and scanning electron microscopy methods. Scanning electron micrographs were obtained using a JEOL 100 CX microscope operated at an accelerating voltage of 20 kV. Samples were gold-coated by evaporation prior to imaging.

Surface areas were measured with a Micromeritics ASAP 2010 system. The monolayer volume of adsorbed N_2 gas is measured from

(15) Deegan, R. D.; Bakajin, O.; Dupont, T. F.; Huber, G.; Nagel, S. R.; Witten, T. A. *Nature* **1997**, *389*, 827–829.

(16) Tian, Z. R.; Tong, W.; Wang, J. Y.; Duan, N.; Krishnan, V. V.; Suib, S. L. *Science* **1997**, *276*, 926–930.

(17) Yang, P.; Zhao, D.; Margolese, D. I.; Chmelka, B. F.; Stucky, G. D. *Nature* **1998**, *396*, 152–155.

(18) Engelkamp, H.; Middelbeek, Nolte, R. J. M. *Science* **1999**, *284*, 785–788.

(19) Barsoum, M. W.; Farber L. *Science* **1999**, *284*, 937–939.

(20) Giraldo, O.; Brock, S. L.; Marquez, M.; Suib, S. L.; Hillhouse, H.; Tsapatsis, M. *Nature* **2000**, *405*, 38.

isotherm data via least-squares fitting of 8 points. About 0.2 g sample is evacuated at 500 μm Hg and then immersed in liquid N_2 .

Electrical conductivities were measured by the dc four-probe method using linear fragments of fibers with lengths of 1 cm and cross sectional areas of $49 \times 10^{-5} \text{ cm}^2$. Silver wires were attached with silver paste to a K-OMS-2 or K-OL-1 fiber. The current was applied along the fiber axis through the external probes and the voltage was measured between the two inner probes.

III. Results and Discussion

A. Synthesis. The resultant TMA_yMnO_x helix has the following theoretical and (experimental) compositions as determined by formulas and inductively coupled plasma and combustion analyses methods, respectively %C 8.82 (10.58), %H 4.36 (4.47), %N 2.57 (2.86). The difference in the organic content may be due to residual TMAOH formed during the synthesis which was not removed after washing the fibers with deionized water. The K-OL-1 helix has a composition of %C 0 (0.34), %H 1.47 (1.23), %N 0 (0.03), K/Mn 0.2325 (0.2325). The K-OMS-2 helix has a K/Mn of 0.2325 (0.2325).

Sols of tetramethyl ammonium (TMA^+) permanganate salts in 2-butanol/ H_2O when placed in capillaries and heated at 85 °C for 160 h (3 mm i.d. capillary tubes) form helical fibers whose composition (after being washed with water to remove impurities) is $[\text{N}(\text{CH}_3)_4]^{+}_{0.93}\text{Mn}^{4+}_{2.1}\text{Mn}^{3+}_{1.9}\text{O}_7(\text{OH})_{1.03} \cdot 5\text{H}_2\text{O}$ with a manganese average oxidation state (AOS) of 3.52. Figure 1A shows examples of various coiling frequencies of these helices in capillary tubes of various dimensions. Figure 1C shows further examples of ring patterns formed from low concentrations of the sol. We have previously briefly communicated²⁰ that helices and rings form under different conditions. Table 1 summarizes our general findings, and these specific examples show that the pitch of the helices and the thickness of the rings can be varied, primarily by controlling the initial concentration of sol in the capillary tube and the diameter and length of the tube.

The diameters of these helices can range from the mm range down to $<30 \mu\text{m}$ with lengths as long as 25 cm. At lower concentrations [10^{-3} M] rings are formed. Helices can be removed from the tubes either by cutting the tube or by flushing the tube with a solution of KNO_3 . Treatment with water does not remove the organic ion. The sizes and number of windings of the helices both show good reproducibility in multiple experiments. Trace levels of silicon are detected at the surface, indicative of surface bonding to the glass capillary. The angle of the tube from a strictly vertical position is not critical, but a horizontal orientation does not lead to well-formed helices.

B. Formation Process. The initially formed amorphous sol precursor has been characterized by small-angle neutron scattering to have homogeneous particle sizes on the order of 4–6 nm. In all syntheses, only one helix is produced in each capillary. Time lapse photographs are shown in Figure 2 from the initial sol stage (Figure 2A) up to a period of 160 h for the final helix shown in Figure 2H. The arrows indicate the level of the solvent during thermal treatment at 85 °C. A gel forms during the first 7 h of reaction. A movie of the formation of helices from the initial sol can be found at <http://www.lib.uconn.edu/chemistry/SuibGroup/suibg.html>.

These photographs and movies show that the formation process proceeds first via contraction of the sol–gel due to solvent evaporation with concomitant formation of a clearer phase near the capillary wall. During drying, liquid is expelled from the wet slug as a clearer phase appears close to the capillary wall. The expulsion is partially driven by capillary forces, which continue to reduce the surface area of the slug to minimize its

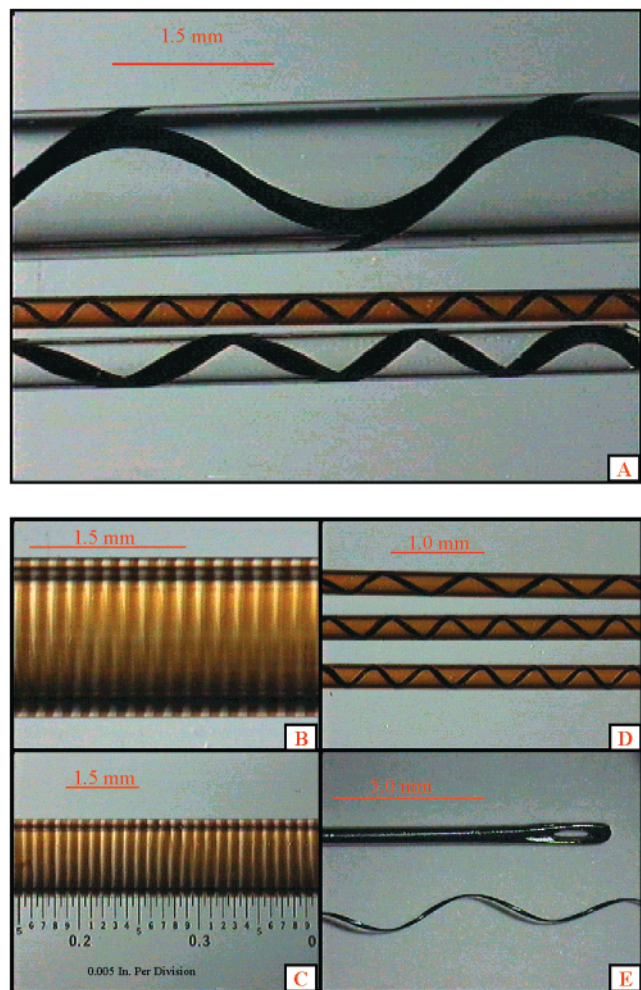


Figure 1. Morphologies of the encapsulated $(\text{TMA})_{0.93}\text{MnO}_x$ products. Final morphologies are observed after solvent evaporation at 85°C . (A) Helices with various coil frequencies. (B) Micro-helix. (C) Micro-parallel rings. (D) Examples of helices with different coil frequencies in similar diameter tubes, i.d. = 0.2 mm. (E) K-OL-1 helix removed from tube.

interfacial energy. However, wetting adhesion between the capillary surface and the slug prevent the slug from completely detaching from the capillary walls. This balance between surface tension and adhesion forces (and gravity, of course) drives the helix formation. The mechanical resistance of the slug toward this helical formation, however, increases with the capillary radius. As a result, slugs with a large diameter are strong enough to detach from the wall. This will provide an upper limit for helix formation. Adhesion of the helix to the walls is an important factor in helix formation since there is a dependence on the size and shape of the container and the chemical characteristics of the surface. For example, square containers did not lead to helix formation. Further evaporation of solvent leads to elimination of capillary pressure, and the gel expands from the lower toward the upper end of the capillary.

A small capillary tube of 1.2 mm i.d. has been magnified and is shown in Figure 1B. This photo clearly shows the well-defined character of the helix and that helices may be formed over a wide range of capillary tube diameters. Figure 1C shows well-ordered rings for sols at lower concentrations than those that produce helices. Figure 1D shows different frequencies of coils in various helices for capillaries of 0.2 mm i.d. Figure 1E shows that these helices can be removed from capillary tubes and retain their helical structure.

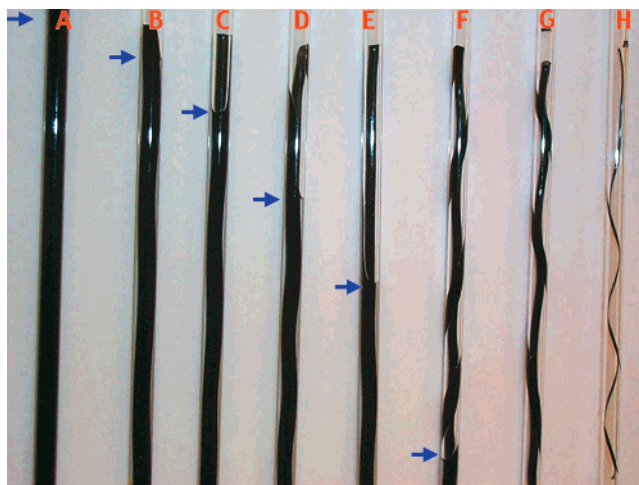


Figure 2. Heating effects of 0.1 M TMA colloidal solutions; tubes of 3 mm i.d. were heated at 85°C for (A) 0 h, (B) 12 h, (C) 17 h, (D) 24 h, (E) 36 h, (F) 67 h, (G) 90 h, (H) 180 h. Blue arrows show the liquid level.

Table 1. Summary of the Effects of [Mn], Capillary Diameters, and Lengths on Morphology

[Mn] (M)	i.d. of the capillary tube (mm)	length of the capillary tube (mm)	result	helical pitch (mm)	ring diameter (mm)
0.10	3.0	180	helix	25	<i>a</i>
0.10	1.2	90	helix	12	<i>a</i>
0.05	1.2	90	helix	6	<i>a</i>
1×10^{-3}	3.0	180	rings	<i>a</i>	0.13
1×10^{-3}	1.2	90	rings	<i>a</i>	0.13

^a Not applicable.

C. Functionalization of Helices by Changing Composition, Porosity, and Structure. The organic cation can be completely removed via ion-exchange and leads to the formation of a layered phase corresponding to synthetic birnessite (OL-1)^{21a} which can be converted via a direct solid-state transformation^{21a} to a microporous tunnel structure.

Ion-exchange of the TMA^+ helix with K^+ leads to helices (Figure 3) having the composition $\text{K}^{+}_{0.93}\text{Mn}^{4+}_{2.1}\text{Mn}^{3+}_{1.9}\text{O}_{7-(\text{OH})_{1.03}} \cdot 2.7\text{H}_2\text{O}$ and an octahedral layered (OL) structure of synthetic birnessite (OL-1).²¹ Lattice parameters derived from X-ray powder diffraction data of Figure 3B are similar to literature reports.²¹ If the helices are crushed into small particles, the OL-1 pattern is still observed, although the preferential orientation of (00 l) reflections is then minimized (note the difference in relative intensities of data of Figure 3 B and C). Optical and electron microscopy photomicrographs show that the external surfaces of the helices are well-formed and uniform, showing smooth surfaces. Fourier transform infrared (FTIR) spectroscopy and microanalyses also show the complete and rapid (10 min, room temperature under ultrasonic cavitation) loss of TMA^+ cations from the helices after ion-exchange with K^+ , suggesting that diffusion is facile and that these materials are permeable.

Thermal treatment of the helices of K-OL-1 at 500°C leads to formation of an octahedral molecular sieve (OMS) tunnel structure of synthetic cryptomelane (OMS-2). An exothermic phase transition of the helical K-OL-1 material was observed via differential scanning calorimetry at 496°C . This phase has

(21) (a) DeGuzman, R. N.; Shen, Y. F.; Suib, S. L.; Shaw, B. R.; O'Young, C. L. *Chem. Mater.* **1993**, *5*, 1395–1400. (b) Shen, Y. F.; Zenger, R. P.; DeGuzman, R. N.; Suib, S. L.; McCurdy, L.; Potter, D. I.; O'Young, C. L. *Science* **1993**, *260*, 511–515.

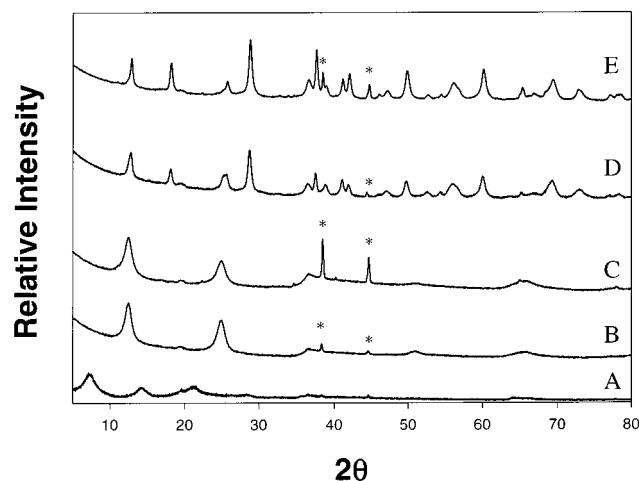


Figure 3. X-ray powder diffraction data²⁹ of (A) TMA_yMnO_x helix, (B) K-OL-1 helix, (C) K-OL-1 ground helix, (D) K-OMS-2 helix, (E) K-OMS-2 ground helix. (*) Reflections from Al sample holder. Lattice parameters for K-OL-1 helix $a = 2.85 \text{ \AA}$; $c = 7.17 \text{ \AA}$; $\gamma = 120^\circ$. Lattice parameters for K-OMS-2 helix space group $I4/m$, $a = 9.848(9) \text{ \AA}$; $c = 2.859(2) \text{ \AA}$.

a composition of $\text{K}^+_{1.86}\text{Mn}^{4+}_{4.7}\text{Mn}^{3+}_{3.3}\text{O}_{14.57}(\text{OH})_{1.43} \cdot 0.7\text{H}_2\text{O}$ with a manganese AOS of 3.58. DSC and TGA studies of the helical K-OMS-2 materials show stability above 800°C . The XRD data clearly show that K-OMS-2 microporous phases²⁹ are present in these helices (Figure 3 D and E). The intensities of the reflections (hkl) with c components that are nonzero are larger for the K-OMS-2 ground sample (Figure 3E) with respect to the K-OMS-2 sample in a fiber form (Figure 3D). This observation is consistent with the c -axis being preferentially along the long axis of the fiber fragment. Figure 4 shows the XRD data collected in a transmission geometry. The uneven intensity distribution of the diffraction rings is further indication of an oriented polycrystalline sample.

The intact helices show a surface area of $2.6 \text{ m}^2/\text{g}$ for the initial OL-1 phase which increases to $13 \text{ m}^2/\text{g}$ for the K-OMS-2 phase. Pore-size distribution data for the K-OMS-2 phase show a peak at 4.4 \AA which is indicative of the presence of the 2×2 tunnel structure of cryptomelane. The HREM data of Figure 5e also show the presence of such tunnels and that the materials are homogeneous. The low surface area of the helices may be indicative of blockage of some of the tunnels by K^+ ions since the $[\text{K}^+]$ is very high, approaching the maximum allowed

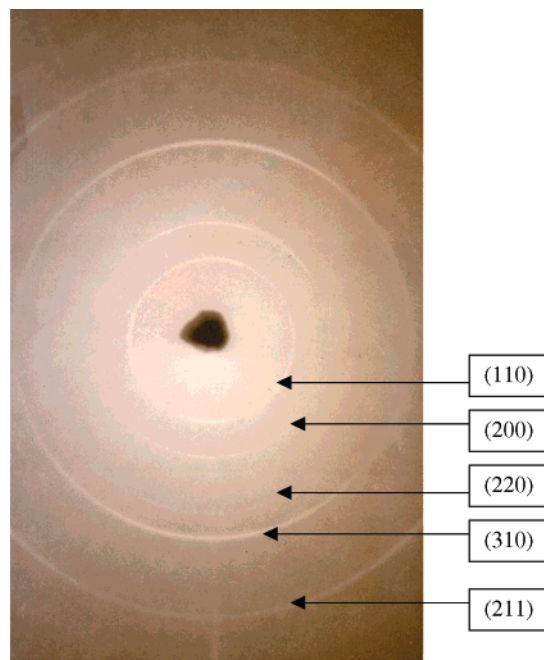


Figure 4. XRD pattern of a K-OMS-2 fiber obtained in transmission mode using $\text{Cu K}\alpha$ radiation.

content. In addition, a density normalized surface area may be important to consider with respect to materials such as silica, alumina, zeolites, or M41-S materials.¹⁶ Finally, this synthetic route of high-temperature conversion to the cryptomelane structure results in lower surface area materials than systems made with more soft approaches.²² Ion-exchange data also suggest that these materials are permeable.

D. Morphology, Microstructure, Conductivity. The morphology and microstructure of the K-OMS-2 helix were examined by scanning and transmission electron microscopy. Figure 5 shows collective results from the microscopic examination of the OMS-2 helices. A small linear fragment of the helix was cut and examined first by SEM. Striations are evident along the length, indicating a fibrous structure further corroborated by the direction of crack propagation from sample preparation (the crack runs along the long axis of the helix fragment, Figure 5b). Secondary spiraling along the radial direction of the helix is shown by the SEM images, Figure 5a

High-resolution SEM images (Figure 5c) indicate that the fragment of the helix consists of elongated crystallites with $0.1 \mu\text{m}$ length and $0.01\text{--}0.03 \mu\text{m}$ width. HRTEM images (Figure 5 d and e) show that the needlelike crystallites have a microporous structure consistent with that of OMS-2 with the channels of the 2×2 octahedra running along the small crystal dimension. HRTEM images also indicate the presence of dislocations in views perpendicular to the c -axis. Electron diffraction patterns are consistent with the OMS-2 structure.

The K-OL-1 precursor helix has an electrical conductivity of $3.7 \times 10^{-4} \Omega^{-1} \text{ cm}^{-1}$ at 21°C . DC 4 probe conductivities of $4.2 \times 10^{-1} \Omega^{-1} \text{ cm}^{-1}$ at 21°C for the K-OMS-2 system are approximately 2 orders of magnitude larger than highly dispersed powder²¹ of K-OMS-2 and ~ 1 order of magnitude higher than most well-formed single crystals of cryptomelane-like materials.²³ In cryptomelane single crystals (AOS = 3.83) the Mn^{3+} ions tend to be ordered and localized close to K^+ ions,²⁴ while in our system the higher content of K^+ ions and lower AOS (3.58) should yield a uniform distribution of Mn^{3+} ions in the crystal lattice, resulting in a situation that enhances the conductivity. Conductivities across the width of the helix

(22) (a) DeGuzman, R. N.; Shen, Y. F.; Neth, E. J.; Suib, S. L.; O'Young, C. L.; Levine, S.; Newsam, J. M. *Chem. Mater.* **1994**, *6*, 815–821. (b) Xia, G. G.; Yin, Y. G.; Willis, W. S.; Wang, J. Y.; Suib, S. L. *J. Catal.* **1999**, *185*, 91–105.

(23) Strobel, P.; Vicat, J.; Qui, D. T. *J. Solid State Chem.* **1984**, *55*, 67–73.

(24) Sato, H.; Enoki, T.; Yamaura, J. I.; Yamamoto, N. *Phys. Rev. B* **1999**, *59*, 12836–12841.

(25) (a) Liesegang, R. E. *Naturwiss. Wochenschr.* **1896**, *II*, 353. (b) Henisch, H. K. *Crystals in Gels and Liesegang Rings*; Cambridge University Press: New York, 1988; p 145–150.

(26) Lu, Y.; Fan, H.; Stump, A.; Ward, T. L.; Roieker, T.; Brinker, C. *J. Nature* **1999**, *398*, 223–226.

(27) Thomas, J. M.; Raja, R.; Sankar, G.; Bell, R. G. *Nature* **1999**, *398*, 227–230.

(28) Yang, P.; Deng, T.; Zhao, D.; Feng, P.; Pine, D.; Chmelka, B. F.; Whitesides, G. M.; Stucky, G. D. *Science* **1998**, *282*, 2244–2246.

(29) XRD patterns (a) TMA_yMnO_x 12.1 \AA (001), 6.2 \AA (002), 4.1 \AA (003), 3.1 \AA (004), 2.4 \AA (100), 1.4 \AA (110). (b), (c) K-OL-1: 7.11 \AA (001), 3.58 \AA (002), 2.47 \AA (100), 1.79 \AA (004), and 1.43 \AA (110). (d), (e) K-OMS-2: 6.973 \AA (110), 4.926 \AA (200), 3.477 \AA (220), 3.112 \AA (310), 2.463 \AA (400), 2.398 \AA (211), 2.326 \AA (330), 2.202 \AA (420), 2.155 \AA (301), 1.932 \AA (510), 1.833 \AA (411), 1.748 \AA (440), 1.687 \AA (530), 1.645 \AA (600), 1.541 \AA (521), 1.432 \AA (002), 1.357 \AA (541), 1.295 \AA (631), 1.238 \AA (402).

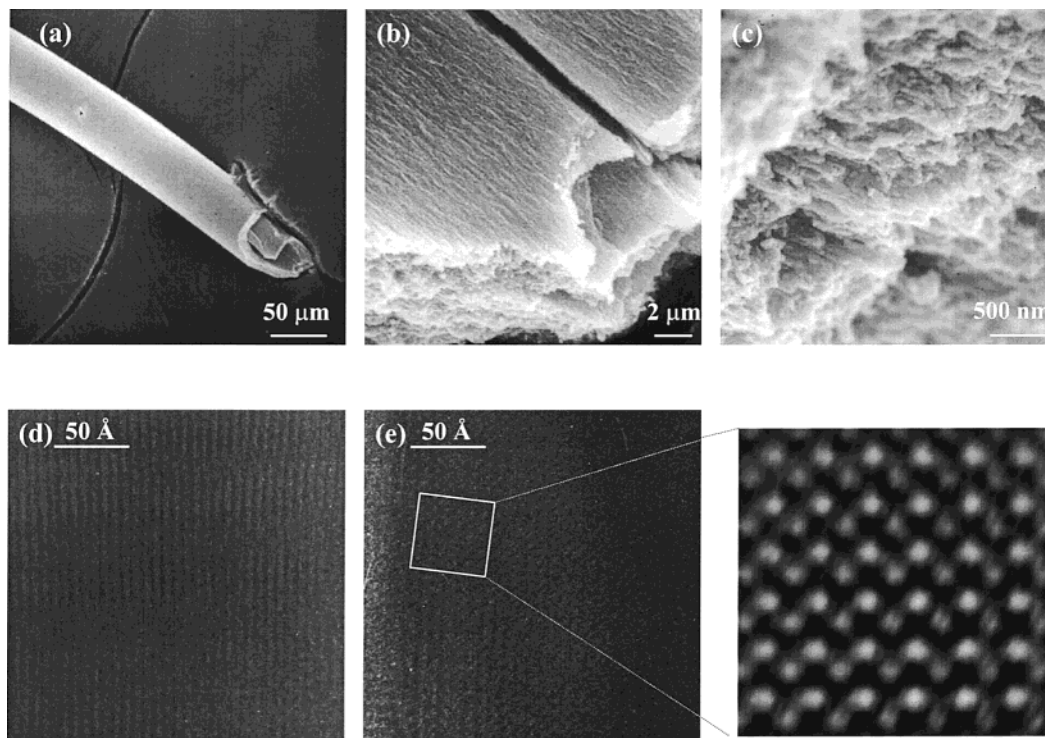


Figure 5. Scanning electron microscopy images of K-OMS-2 fiber fragment (a, b, c) at increasing magnifications from a to c. (d and e) HRTEM views of the crystallites: (d) is a view perpendicular to the long axis of the crystallite (*c*-axis) and (e) is a view down the *c*-axis. The inset of (e) is an FFT processed image showing structure consistent with the 2×2 channel structure of K-OMS-2.

are lower (about 1 order of magnitude) than along the length. The higher conductivity along the length of the helices with respect to bulk powders may be due to the microstructure of the wires. Literature data suggest that the conductivity of synthetic cryptomelane is related to small polaron hopping.²⁴ The hierarchical microstructure [primary microporous crystal structure, secondary mesoscopic assembly of elongated crystallites parallel to each other with their *c*-axis (channel direction) lying along the length of the wire, and tertiary macroscopic spiral-within-helix shape] is formed in the absence of external forces or initially imposed concentration gradients.

The resulting microstructure leads to the formation of porosity on several scales: (1) microporosity of the 2×2 crystal structure of OMS-2, (2) mesoporosity between the colloidal crystallites, and (3) macroporosity between the winding of the helix and to a net alignment and connectivity of the microporous network along the length of the helix. This alignment leads to conduction along the wire, and as a result of the porosity, rate processes such as ion exchange are enhanced due to fast diffusion.

Syntheses with capillaries or other surfaces that have been coated to remove OH groups on the walls or Teflon tubes lead to distorted helical or nonhelical structures. Both right- and left-handed helices are observed in these syntheses with about the same amount of each. When invasive objects or deposits are introduced, the direction of the winding of the helix can be altered. The wires can be wound around another object without breakage or collapse of the wires. The flexibility of such helices is likely due to the interlocking fibers that run along the length of the helices.

The sizes of the helices are directly controlled by the [Mn] in the sol precursors and by the diameters of the capillary tubes. However, capillaries are not required to form these phases. When a beaker is used, the wire attaches to the surface and winds around the inner surface of the beaker. These wires grow

as a continuous filament. However, exactly how these particulates organize in the helical structures is not well-known. A self-assembly process resulting in evenly spaced turns of the helices or of the rings might be in effect. Low concentrations of the sol when deposited on the surface lead to well-ordered micropatterns of lines down to about $1 \mu\text{m}$.

The results described above clearly demonstrate the ability to reproducibly create a wire exhibiting order across multiple-length scales (from the nm to cm scale) starting from a well-mixed colloidal precursor and applying no external forces other than its confinement in a capillary or beaker and heating for a period of time.

Reproducible formation of helices in gradient-free rather than Liesegang (gradient) systems²⁵ by self-organization from the whole volume of the system has not been reported before. The affinity of colloidal particles to nucleate at the capillary wall is certainly a major factor; however, formation of helical fragment-(s) requires genuine symmetry breaking^{25b} since it cannot be imposed from boundaries of the capillary.

Ozin et al.^{13b} have mathematically modeled observations of helix formation and transverse and longitudinal differential contraction processes for helices of hexagonal mesoporous silica from mesoporous films. While such a model may provide some of the explanation of manganese oxide helices described here, it is clear that other factors in our system play a major role such as confinement in the capillary tube, composition of the capillary wall, a strong solvent dependency, and other parameters.

Microscopy studies show that there is an anchoring of the sols and gels to the walls of the tube during growth. Preferred orientation noted in XRD along with electron microscopy data suggests that OH groups of the capillary walls interact with OH groups of the sol to form layered phases parallel to the wall and tunnels in OMS-2 helices that run along the helix. Time lapse photographs indicate contraction followed by expansion

along the length of the capillary. The helix form is clearly observed during the expansion.

One can envision the helix formation as a result of periodic expansion due to stress development during growth. Despite the uncertainties in the operating mechanism(s), the results reported here establish the potential for reproducible formation of hierarchically ordered functional materials and macrostructures starting from a well-mixed precursor phase and relying solely on self-organization.

IV. Conclusions

These systems may yield new generations of materials of wide-ranging composition due to ready ion exchange. The materials can be thermally modified to produce OL and OMS phases and provide templates for a variety of potential applications. Modeling and experimental studies are in progress in order to more fully understand the origin of the helices and rings, which are believed to be formed in 3D and 2D processes, respectively.

Current investigations include novel syntheses of mesostructures,²⁶ use of such helices, rings, and wires in lithography, as sensors, new battery materials, in catalytic oxidations of hydrocarbons,²⁷ in shape-selective reactions, and for chromato-

graphic separations. Hierarchically ordered mixed-valent transition metal oxide materials of our systems can likely be prepared.²⁸ Semiconducting fibers might lead to new circuitry materials if the sizes can be limited to diameters lower than 1 micrometer. Other related forms such as films and lines may be more useful in this regard.

Unique features of these systems include the unusual helical morphology, conductivity, ease of ion-exchange, transformations to alternate structures while preserving the morphology and wire-like properties, and adsorption properties, which are due to the generation of hierarchical porous structures.

Acknowledgment. This research was supported by the U.S. Department of Energy, Office of Basic Energy Sciences, Division of Chemical Sciences. The authors thank Professor James Knox for the XRD transmission measurements. O.G. acknowledges the support of Colciencias, Colombia. M.T. acknowledges support from the David and Lucile Packard Foundation. We acknowledge L. Iton of Argonne National Labs, C. Chang of Notre Dame, and D. Weitz of Harvard for helpful discussions.

JA0018872